

Journal of Materials Chemistry A

Accepted Manuscript



This is an *Accepted Manuscript*, which has been through the Royal Society of Chemistry peer review process and has been accepted for publication.

Accepted Manuscripts are published online shortly after acceptance, before technical editing, formatting and proof reading. Using this free service, authors can make their results available to the community, in citable form, before we publish the edited article. We will replace this *Accepted Manuscript* with the edited and formatted *Advance Article* as soon as it is available.

You can find more information about *Accepted Manuscripts* in the [Information for Authors](#).

Please note that technical editing may introduce minor changes to the text and/or graphics, which may alter content. The journal's standard [Terms & Conditions](#) and the [Ethical guidelines](#) still apply. In no event shall the Royal Society of Chemistry be held responsible for any errors or omissions in this *Accepted Manuscript* or any consequences arising from the use of any information it contains.

Electrochemical properties of all-solid-state lithium batteries with
amorphous MoS₃ electrodes prepared by mechanical milling

Takuya Matsuyama¹, Akitoshi Hayashi^{1,*}, Tomoatsu Ozaki², Shigeo Mori² and Masahiro

Tatsumisago¹

¹ Department of Applied Chemistry, Graduate School of Engineering, Osaka Prefecture University,
1-1 Gakuen-cho, Naka-ku, Sakai, Osaka 599-8531, Japan

² Department of Materials Science, Graduate School of Engineering, Osaka Prefecture University,
1-1 Gakuen-cho, Naka-ku, Sakai, Osaka 599-8531, Japan

*** Corresponding author**

Akitoshi Hayashi (associate professor)

Tel./fax: +81 72 254 9334

E-mail address: hayashi@chem.osakafu-u.ac.jp

Keywords

molybdenum sulfide, all-solid-state battery, lithium battery, mechanical milling, amorphous

Abstract

Amorphous molybdenum trisulfide (MoS_3) active materials were successfully prepared by ball milling of the mixture of Mo metal and sulfur. The atomic ratio of Mo to S in the starting mixture was 1:3. All the diffraction peaks due to Mo metal and sulfur disappeared in the milled sample. In addition to a halo pattern due to the amorphous structure, it is a broad peak at about 15° that appeared in the diffraction profile obtained in MM 80 hours. The HR-TEM image revealed that microstructure of the milled sample was characterized as random distribution of nano-sized domains with the size of 2 ~ 3 nm, which consist of crystalline MoS_2 with the layered structure. The DTA curve of the amorphous MoS_3 exhibited no endothermic peaks attributable to melt of crystalline sulfur. The particle size of the amorphous MoS_3 was about 1 μm . The milled samples were not formed by agglomeration of submicron-sized ordinary particles. The all-solid-state lithium secondary batteries using a sulfide solid electrolyte and the amorphous MoS_3 electrode showed capacities higher than 670 mAh g^{-1} for 60 cycles. The amorphous MoS_3 had a higher capacity than the cell using the crystalline MoS_2 .

Introduction

Lithium-ion batteries are widely used in portable electronic devices such as cell phones and personal computers.^{1,2} Increasingly they are also being scaled up for using large applications in electric vehicles and smart grids.³ However, due to limited capacity in both positive and negative electrodes, the specific energy density of lithium-ion batteries needs to improve remarkably to meet the requirements for practical applications.⁴ Current positive electrode materials have an actual capacity less than half that of negative electrode materials such as graphite and silicon. Therefore, high-capacity positive electrode materials are required to realize lithium-ion batteries with higher-energy densities.

Sulfur is one of the most promising positive electrode materials because of its high theoretical specific capacity of 1672 mAh g^{-1} , which is at least 5 times higher than that of the transition metal oxides such as LiCoO_2 .^{5,6} Sulfur also has many other advantages of low cost, abundant resource and environmental friendliness. However, fast capacity fading during cycling of Li/S batteries has been a major challenge toward its practical use.^{7,8} The poor cycle life is due to the dissolution of intermediate lithium polysulfides, which are formed during the battery operation, into organic liquid electrolytes, the volumetric expansion and contraction of sulfur during cycling and the insulating nature of sulfur and lithium sulfide. A well-designed sulfur electrode to clear these issues is required. The current approaches focus on confining sulfur active materials in porous nanostructures to

capture the lithium polysulfides during charge-discharge reactions.⁹⁻¹² The cycle life and utilization of Li/S batteries are drastically improved by maintaining an electron conducting path to the sulfur active materials and physically inhibiting the dissolution of polysulfides into liquid electrolytes. Although an excellent structural electrode design mentioned above has led to the outstanding electrochemical performances, there are still a few soluble species escaping from the nanostructures as a matrix over numerous cycles, resulting in a consecutive capacity fading with cycling.

For fundamental improvement in inhibiting the dissolution of lithium polysulfides, the use of inorganic solid electrolytes instead of organic liquid electrolyte is an effective approach. Various inorganic solid electrolytes such as $\text{Li}_2\text{S-SiS}_2$ glass,¹³ $\text{Li}_2\text{S-P}_2\text{S}_5$ glass-ceramics^{14, 15} and thio-LISICONs in $\text{Li}_4\text{GeS}_4\text{-Li}_3\text{PS}_4$ system¹⁶ with high Li^+ ion conductivity of over $10^{-4} \text{ S cm}^{-1}$ at 25 °C have been explored as electrolytes in all-solid-state lithium batteries. Recent reports have described that sulfide-based solid electrolytes such as $\text{Li}_{10}\text{GeP}_2\text{S}_{12}$ crystals and $70\text{Li}_2\text{S}\cdot30\text{P}_2\text{S}_5$ glass-ceramics have high lithium-ion conductivity of $1.2\times10^{-2} \text{ S cm}^{-1}$ ¹⁷ and $1.7\times10^{-2} \text{ S cm}^{-1}$ ¹⁸, respectively, at room temperature. Those values are as high as the conductivity of conventional organic liquid electrolytes. The Li/S cells using these solid electrolytes exhibited a good cycling performance because of completely eliminating the issue of polysulfides dissolution.¹⁹⁻²² Several attempts have been made to enhance utilization of sulfur active materials. For instance, composites of sulfur and electrically conducting materials such as copper^{19, 23, 25} or nanocarbon^{22, 25} were

prepared by mechanical milling^{19, 23, 24} and gas-phase mixing.²² Furthermore, the construction of not only an electron conducting path but also a Li^+ ion conducting path to the sulfur active material is essential for improving the performance in all-solid-state Li/S batteries. Recently, we found that mechanical milling of a mixture of sulfur or Li_2S active material, acetylene black (AB) and $\text{Li}_2\text{S-P}_2\text{S}_5$ solid electrolytes (SE) is powerful approach for enhancing the reversible capacity and the rate capability in all-solid-state Li/S batteries.²⁶ Lin *et al.* reported that sulfur-rich $\text{Li}_3\text{PS}_{4+n}$ prepared by the solution process using THF was applied to all-solid-state cells and they showed good electrochemical performance.^{27,28}

In this paper, we focus on a transition metal sulfide with a higher electronic conductivity than that of sulfur. The sulfide electrode active materials with high electronic conductivity and capacity can be prepared by combining sulfur and transition metal sulfides. These sulfide positive electrodes will be compatible with sulfide solid electrolytes in all-solid-state batteries with sulfide-sulfide interfaces. The use of molybdenum disulfide (MoS_2) as positive electrode active materials for lithium batteries is of great interest because of its low cost and high safety.²⁹ The lithium batteries with MoS_2 showed high reversible capacity with excellent cyclability. Sulfur-rich molybdenum sulfide would have higher capacity than the MoS_2 crystal. Moreover, sulfur-rich molybdenum sulfide electrodes would have higher electronic conductivity than that of sulfur. This charge-discharge reaction is affected by the presence of additional sulfur atoms in the sulfur-rich molybdenum sulfide

electrode.

We reported that amorphous TiS_3 prepared by ball milling had better cyclability than crystalline TiS_3 .^{30, 31} Moreover, the first discharge capacity of the all-solid-state cell with amorphous TiS_3 exhibited approximately 400 mAh g^{-1} , which is higher than the initial capacity of the liquid type cell with crystalline TiS_3 (*ca.* 350 mAh g^{-1})^{30, 31} as described above. These results suggested that amorphous sulfur-rich titanium sulfide (*a*- TiS_3) showed the higher reversible capacity.

Electrode properties of amorphous MoS_3 (*a*- MoS_3) prepared by pyrolysis of $(\text{NH}_4)_2\text{MoS}_4$ have been investigated in an organic liquid electrolyte.³² A liquid-type cell with *a*- MoS_3 electrode shows the reversible capacity of 400 mAh g^{-1} . Although crystalline MoS_3 has not been synthesized so far, *a*- MoS_3 electrode active materials have a higher reversible capacity than that of crystalline MoS_2 . All-solid-state lithium batteries with *a*- MoS_3 electrode active materials have not been reported yet.

Amorphization of active materials is potentially capable of achieving higher capacity and cyclability because of open and random structure in amorphous materials. For example, amorphous V_2O_5 and MoO_2 were reported to exhibit better rechargeability than crystalline V_2O_5 or MoO_2 did.³³
³⁴ A coin-type cell with amorphous MoO_2 electrode showed particularly higher capacity and better rate capability than that of the cell with crystalline MoO_2 .³⁴ Ku *et al.* reported that the cell performance was improved because the structural defects in amorphous MoO_2 acted as a Li^+ storage site. Sakuda *et al.* reported that the all-solid-state cells with amorphous TiS_4 and amorphous NbS_x

showed high reversible capacities.³⁵⁻³⁷ Thus, the amorphous electrode active materials are very attractive.

In this study, amorphous MoS₃ was successfully prepared by mechanical milling from the mixtures of molybdenum metal and sulfur. Both microstructures and electrochemical properties of amorphous MoS₃ in all-solid-state cells with sulfide solid electrolytes were investigated. Electrochemical performances in amorphous MoS₃ and crystalline MoS₂ positive electrodes in all-solid-state cells were examined. It is revealed that amorphous MoS₃ had a higher capacity and superior cyclability.

Experimental

Amorphous MoS₃ electrode active materials were prepared by mechanical milling. Reagent-grade Mo metal (99.9+%; Aldrich) and sulfur (99.98%; Aldrich) were used as starting materials. The atomic ratio of Mo to S in the starting mixture was 1:3. The mixture of these materials was mechanically milled at ambient temperature using a planetary ball mill apparatus (Pulverisette 7; Fritsch) with a zirconia pot (volume of 45 ml) and 500 zirconia balls (4 mm diameter). The rotational speed was set to 370 rpm. The milling time was 80 hours. To examine crystal structures of prepared samples, X-ray diffraction experiment was carried out using a X-ray diffractometer (UltimaIV; Rigaku). Differential thermal analysis (DTA) was performed by using a thermal analyzer

(Thermo Plus TG8110; Rigaku) at a heating rate of $10^{\circ}\text{C min}^{-1}$. The morphology of the amorphous MoS_3 was examined using a scanning electron microscopy (SEM, JSM-6610A; JEOL) and a transmission electron microscope (TEM, JEM-2100F; JEOL).

All-solid-state electrochemical cells were fabricated as follows. The $80\text{Li}_2\text{S}\cdot 20\text{P}_2\text{S}_5$ (mol%) solid electrolyte was prepared by the mechanical milling and then heated at 210°C for 1 h.¹⁴ The lithium ion conductivity of the solid electrolyte was $1.3 \times 10^{-3} \text{ S cm}^{-1}$ at 25°C .¹⁵ The amorphous MoS_3 prepared by milling and the crystalline MoS_2 (99%; Aldrich) were used as active materials. The working electrode was prepared by mixing of the active materials, the $80\text{Li}_2\text{S}\cdot 20\text{P}_2\text{S}_5$ solid electrolyte and acetylene black with the weight ratio of 40:60:6. The solid electrolyte and acetylene black were respectively added to secure lithium-ion and electron conduction paths to the active material in the working electrode. The obtained working electrode (10 mg) and the solid electrolyte (80 mg) were placed in polycarbonate tube (10 mm diameter) and pressed together under 360 MPa. A Li-In alloy was put on the solid electrolyte layer as a counter-reference electrode. Then pressure of 120 MPa was applied to the three-layered pellet. Finally, two electrode cells sandwiched with two stainless-steel disks as a current collector were obtained. All processes described above were conducted in a dry Ar glove box. The electrochemical tests were conducted at 25°C in an Ar-filled atmosphere using a charge-discharge measuring device (BTS-2004; Nagano Co.).

Results and discussion

Figure 1 shows the X-ray diffraction profiles of the molybdenum sulfide prepared by milling of the mixtures of Mo and S at various milling periods of time. In the mixtures, the diffraction peaks belonging to the starting materials, Mo metal and sulfur, were detected. The diffraction peaks due to octahedral ring structure of sulfur disappeared by milling for 20 hours. On the other hand, the intensities of the diffraction peaks due to Mo metal gradually decreased as the milling time is longer. After milling for 80 hours, all the diffraction peaks due to Mo metal and sulfur disappeared. In addition to a halo pattern due to the amorphous structure, it is a broad peak at about 15° that appeared in the diffraction profile obtained in MM 80 hours. We analyzed the position of the broad peak around 15° and found that the position corresponds to the (002) diffraction peak of crystalline MoS_2 (JCPDS N0. 070-9264). Thus, to clarify microstructures in some milled materials, high-resolution TEM observation was conducted. Figure 2 shows (a) a high-resolution TEM image, (b) electron diffraction pattern and (c) its intensity profile of the molybdenum sulfide prepared by milling for 80 hours. The inset in (a) shows magnified image of (a). The HR-TEM image revealed that microstructure in the milled sample was characterized as random distribution of nano-sized domains with the size of $2 \sim 3$ nm, which consist of crystalline MoS_2 with the layered structure. Note that lattice spacing due to the (002) plane of crystalline MoS_2 was approximately 6 \AA , which was almost coincident with spacing of the lattice fringes in Fig. 2 (a). Electron diffraction patterns

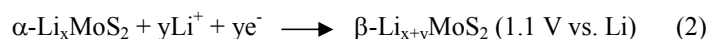
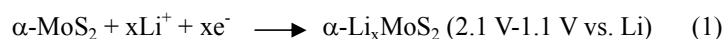
obtained in the milled sample showed debye rings without diffraction spots. Figure 2 (c) shows the intensity profile obtained along the dotted line in the ED pattern of Fig. 2 (b) and the origin at the horizontal axis corresponds to the direct 000 spot. The peak positions of the intensity profile almost corresponded to those of crystalline MoS₂. From these considerations, it is suggested that the prepared sample should include clusters consisting of MoS₂ with the layered structure. It is noted that the prepared material including the clusters is called amorphous MoS₃ in the following discussion.

The DTA curve of the sample milled for 80 hours exhibited no endothermic peaks attributable to melt of crystalline sulfur whereas endothermic peaks were observed at around 115°C in the DTA curve obtained in the mixture of Mo metal and S before milling (0 hour), as shown in Fig. 3. This implies that chemical reaction between Mo metal and sulfur occurred completely.

The SEM images of the sample before and after milling are shown in Fig. 4. The SEM image of the mixture of Mo metal and S before mechanical milling indicated that the mixture consisted of Mo metal particles of *ca.* 20 μm in size and sulfur particles of *ca.* 100 μm. After milling for 80 hours, the milled sample consisted of submicron-sized particles. The starting materials as Mo metal and sulfur particles were not observed.

Figure 5 shows (a) the charge–discharge curves and (b) the rate performance of all-solid-state cells Li–In/80Li₂S·20P₂S₅ glass-ceramic/amorphous MoS₃ or crystalline MoS₂. In Fig. 5 (a),

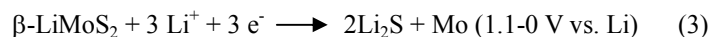
charge–discharge measurements of the cells were conducted at the current density of 0.064 mA cm⁻² (C/50) at 25°C. The right side ordinate axis represents the electrode potential vs. Li⁺/Li, as calculated based on the potential difference between the Li–In and Li electrode (0.62 V). The Li–In alloy was used as a counter electrode, because Li–In alloy exhibits a stable voltage plateau at 0.62 V vs Li⁺/Li in an all-solid-state cell using a sulfide solid electrolyte.³⁸ The first discharge capacity of the cell using crystalline MoS₂ was approximately 270 mAh g⁻¹. The obtained discharge capacity was larger than 167 mAh g⁻¹ (the capacity corresponding to the insertion of 1 molar Li to MoS₂). MoS₂ crystal was practically used as the positive electrode in lithium metal batteries with liquid organic electrolyte.²⁹ Electrochemical reaction mechanism of crystalline MoS₂ with lithium is reported as follows:



The intercalation reaction of Li⁺ ions to α -MoS₂ was observed at the potential range of 2.1–1.1 V vs. Li in the initial discharge process. The discharge plateau due to the two phase reaction between α -MoS₂ and β -MoS₂ appeared at 1.1 V vs. Li. The charge-discharge reaction after the initial discharge process proceeded in β -MoS₂ because the structure change to α -MoS₂ did not occur.²⁹ Recently, Du *et al.* and Fang *et al.* reported that the cell with MoS₂ crystal exhibited a higher capacity of approximately 670 mAh g⁻¹ (the capacity corresponding to the insertion of 4 molar Li to

MoS₂) than 167 mAh g⁻¹.^{39,40} The following reaction is suggested on the discharge process to 0 V vs.

Li:



The all-solid-state cell with crystalline MoS₂ showed a higher capacity than 167 mAh g⁻¹ because the excess Li⁺ would react with β-LiMoS₂ due to the reaction (3) occurring at the potential range of 1.1-0 V vs. Li. Because the discharge cut-off voltage was 0.62 V vs. Li, the all-solid-state cell did not show a higher discharge capacity than the cell with an organic electrolyte reported by Du *et al.* and Fang *et al.* The initial charge capacity was about 180 mAh g⁻¹. The initial coulombic efficiency of the cell with crystalline MoS₂ was 69.3%. This capacity was close to 167 mAh g⁻¹. Additionally, the charge-discharge curve of the all-solid-state cell with crystalline MoS₂ was similar to that of the cell using an organic liquid electrolyte, suggesting that electrochemical reaction mechanism of the crystalline MoS₂ electrode in all-solid-state cells is almost the same as that in the cell with an organic liquid electrolyte.

On the other hand, the amorphous MoS₃ (*a*-MoS₃) electrode in the all-solid-state cell with the sulfide solid electrolyte exhibited higher capacity and better cyclability, compared to the crystalline MoS₂ in the all-solid-state cell. The initial discharge and charge capacities of the cell with *a*-MoS₃ were about 760 mAh g⁻¹ and 720 mAh g⁻¹, respectively. The initial coulombic efficiency of the cell using *a*-MoS₃ was 93.4%. The obtained discharge capacity was higher than 670 mAh g⁻¹ (the

capacity corresponding to the insertion of 4 molar Li to MoS₂). The capacity loss was observed at the second cycle and a possible reason for it is a partial contact loss in the working electrode by a volume change of *a*-MoS₃. The cell maintained the capacity of about 670 mAh g⁻¹ up to the 10th cycle. The cell with *a*-MoS₃ did not show well-defined discharge plateaus and this is a typical behavior of amorphous electrode materials. Cyclic voltammogram (CV) of the cell is shown in a supplemental figure (Fig. S1) and three broad peaks observed in CV almost corresponded to the discharge profile as shown in Fig. 5 (a). The discharge potential of the cell using *a*-MoS₃ was higher than that of the cell using crystalline MoS₂. This suggested that the additional sulfur reacted with Li⁺ during discharge process to 1.6 V vs. Li. The electrochemical reaction at *ca.* 2.0 V vs. Li at the initial discharge process would be based on the additional sulfur redox because this electrochemical potential was similar to that of elemental sulfur. The electrochemical reaction mechanism of the amorphous MoS₃ below 1.6 V vs. Li is similar to that of MoS₂.

The rate performance of the cells with *a*-MoS₃ and crystalline MoS₂ are shown in Fig. 5 (b). The cell using MoS₂ showed the reversible capacity about 180 mAh g⁻¹ for 10 cycles at the current density of 0.064 mA cm⁻². The reversible capacity decreased gradually with increasing the current density. The reversible capacity of the cell with crystalline MoS₂ exhibited about 75 mAh g⁻¹. On the other hand, the cell with *a*-MoS₃ showed the higher reversible capacity than the cell with MoS₂. The reversible capacity of the cell using *a*-MoS₃ was about 670 mAh g⁻¹ for 10 cycles at the current

density of 0.064 mA cm^{-2} . After the 2nd cycle, the coulombic efficiency of the cell was about 100%. The capacity fading was not observed with increasing the current density from 0.064 mA cm^{-2} to 0.13 mA cm^{-2} . However, the reversible capacity of the cell with *a*-MoS₃ was about 400 mAh g^{-1} at the current density of 1.3 mA cm^{-2} . This suggests that sulfur-rich molybdenum sulfide electrode active materials have higher reversible capacity than the MoS₂ crystal even at the high current density. Structure analyses for *a*-MoS₃ are needed to clarify reaction mechanism and will be done in the near future.

Conclusions

Amorphous MoS₃ was successfully prepared by ball milling of the mixture of Mo metal and sulfur. The present XRD, DTA, SEM and HR-TEM experiments revealed that amorphous MoS₃ is characterized by the random distribution of the nano-sized domains consisting of clusters of crystalline MoS₂. The initial discharge capacity of the all-solid-state cell with the amorphous MoS₃ was approximately 760 mAh g^{-1} . The capacity was higher than 670 mAh g^{-1} (the capacity corresponding to the insertion of 4 molar Li to MoS₂). The cell with amorphous MoS₃ electrode retained discharge capacity of about 670 mAh g^{-1} for 60 cycles. The amorphous MoS₃ had higher capacity than the crystalline MoS₂.

Acknowledgments

This research was financially supported by JST ALCA-SPRING project.

References

1. J. M. Tarascon and M. Amand, *Nature*, 2001, **414**, 359-367.
2. M. Amand and J. M. Tarascon, *Nature*, 2008, **451**, 652-657.
3. B. Dunn, H. Kamath and J. M. Tarascon, *Science*, 2011, **334**, 928-935.
4. J. B. Goodenough and Y. Kim, *Chem. Mater.*, 2010, **22**, 587-603.
5. H. Yamin, A. Gorenshtein, J. Penciner, Y. Sternberg and E. Peled, *J. Electrochem. Soc.*, 1988, **135**, 1045-1048.
6. B.H. Jeon, J.H. Yeon, K.M. Kim and I.J. Chung, *J. Power Sources*, 2002, **109**, 89-97.
7. R.D. Rauh, K.M. Abraham, G.F. Pearson, S.K. Surprenant and S.B. Brummer, *J. Electrochem. Soc.*, 1979, **126**, 523-527.
8. H. Yamin and E. Peled, *J. Power Sources*, 1983, **9**, 281-287.
9. X. Ji and L. F. Nazar, *J. Mater. Chem.*, 2010, **20**, 9821-9826.
10. L. Yuan, H. Yuan, X. Qiu, L. Chen and W. Zhu, *J. Power Sources*, 2009, **189**, 1141-1146.
11. B. Zhang, C. Lai, Z. Zhou and X. P. Gao, *Electrochim. Acta*, 2009, **54**, 3708-3713.

12. X. Ji, K. T. Lee and L. F. Nazar, *Nat. Mater.*, 2009, **8**, 500-506.
13. A. Pradel and M. Ribes, *Solid State Ionics*, 1986, **18–19**, 351-355.
14. A. Hayashi, S. Hama, T. Minami and M. Tatsumisago, *Electrochem. Commun.*, 2003, **5**, 111-114.
15. F. Mizuno, A. Hayashi, K. Tadanaga and M. Tatsumisago, *Solid State Ionics*, 2006, **177**, 2721-2725.
16. R. Kanno and M. Murayama, *J. Electrochem. Soc.*, 2001, **148**, A742-A746.
17. N. Kamaya, K. Homma, Y. Yamakawa, M. Hirayama, R. Kanno, M. Yonemura, T. Kamiyama, Y. Kato, S. Hama, K. Kawamoto and A. Mitsui, *Nat. Mater.*, 2011, **10**, 682–686.
18. Y. Seino, T. Ohta, K. Takada, A. Hayashi and M. Tatsumisago, *Energy Environ. Sci.*, 2014, **7**, 627-631.
19. A. Hayashi, T. Ohtomo, F. Mizuno, K. Tadanaga and M. Tatsumisago, *Electrochem. Commun.*, 2003, **5**, 701-705.
20. A. Hayashi, T. Ohtomo, F. Mizuno, K. Tadanaga and M. Tatsumisago, *Electrochim. Acta*, 2004, **50**, 893-897.
21. N. Machida, K. Kobayashi, Y. Nishikawa and T. Shigematsu, *Solid State Ionics*, 2004, **175**, 247-250.
22. T. Kobayashi, Y. Imade, D. Shishihara, K. Homma, M. Nagao, R. Watanabe, T. Yokoi, A.

- Yamada, R. Kanno and T. Tatsumi, *J. Power Sources*, 2008, **182**, 621-625.
23. N. Machida and T. Shigematsu, *Chem. Lett.*, 2004, **33**, 376-377.
24. A. Hayashi, R. Ohtsubo, T. Ohtomo, F. Mizuno and M. Tatsumisago, *J. Power Sources*, 2008, **183**, 422-426.
25. T. Takeuchi, H. Kageyama, K. Nakanishi, M. Tabuchi, H. Sakaebe, T. Ohta, H. Senoh, T. Sakai and K. Tatsumi, *J. Electrochem. Soc.*, 2010, **157**, A1196-A1201.
26. M. Nagao, A. Hayashi and M. Tatsumisago, *Electrochim. Acta*, 2011, **56**, 6055-6059.
27. Z. Lin, Z. Liu, W. Fu, N. J. Dudney and C. Liang, *Angew. Chem. Int. Ed.*, 2013, **52**, 7460-7463.
28. Z. Lin, Z. Liu, N. J. Dudney and C. Liang, *ACS Nano*, 2013, **7**, 2829-2833.
29. M. A. Py and R. R. Haering, *Can. J. Phys.*, 1983, **61**, 76-84.
30. A. Hayashi, T. Matsuyama, A. Sakuda and M. Tatsumisago, *Chem. Lett.*, 2012, **41**, 886-888.
31. T. Matsuyama, A. Sakuda, A. Haysahi, Y. Togawa, S. Mori and M. Tatsumisago, *J. Solid State Electrochem.*, 2013, **17**, 2697-2701.
32. J. J. Auburn, Y. L. Barberio, K. J. Hanson, D. M. Schleigh, M. J. Martin, *J. Electrochem. Soc.*, 1987, **134**, 580-586.
33. N. Machida, R. Fuchida and T. Minami, *J. Electrochem. Soc.*, 1989, **136**, 2133-2136.
34. J. H. Ku, J. H. Ryu, S. H. Kim, O. H. Han and S. M. Oh, *Adv. Funct. Mater.*, 2012, **22**, 3658-3664.

35. A. Sakuda, N. Taguchi, T. Takeuchi, H. Kobayashi, H. Sakaebe, K. Tatsumi and Z. Ogumi, *Electrochem. Commun.*, 2013, **31**, 71-75.
36. A. Sakuda, N. Taguchi, T. Takeuchi, H. Kobayashi, H. Sakaebe, K. Tatsumi and Z. Ogumi, *Solid State Ionics*, 2014, **262**, 143-146.
37. A. Sakuda, N. Taguchi, T. Takeuchi, H. Kobayashi, H. Sakaebe, K. Tatsumi and Z. Ogumi, *Electrochem. Lett.*, 2014, **3**, A79-A81.
38. K. Takada, N. Aotani, K. Iwamoto and K. Kondo, *Solid State Ionics*, 1996, **86-87**, 877-882.
39. G. Du, Z. Guo, S. Wang, R. Zeng, Z. Chen and H. Liu, *Chem. Commun.*, 2010, **46**, 1106-1108.
40. X. Fang, C. Hua, X. Guo, Y. Hu, Z. Wang, X. Gao, F. Wu, J. Wang and L. Chen, *Electrochim. Acta*, 2012, **81**, 155-160.

Figure captions

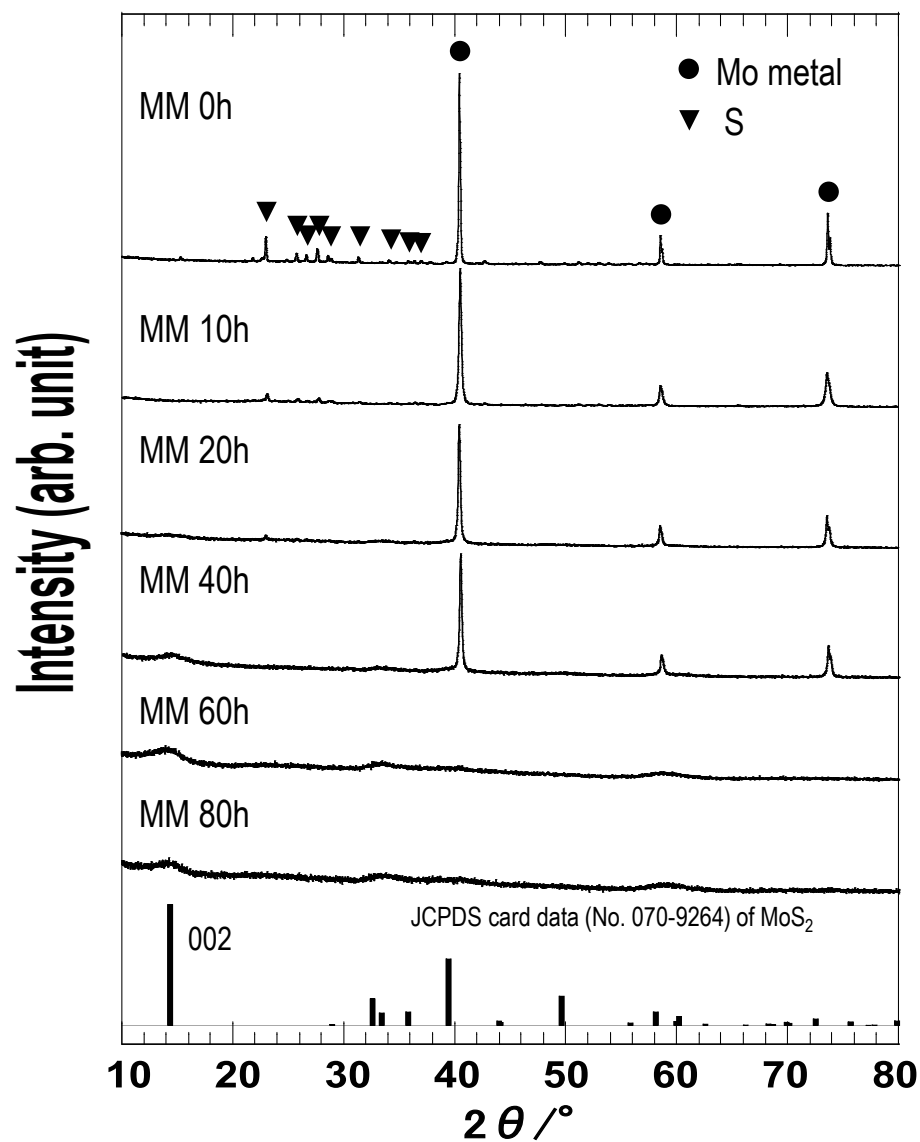
Figure 1 XRD profiles of the mixture products prepared by mechanical milling (MM) of Mo metal and sulfur for different periods time.

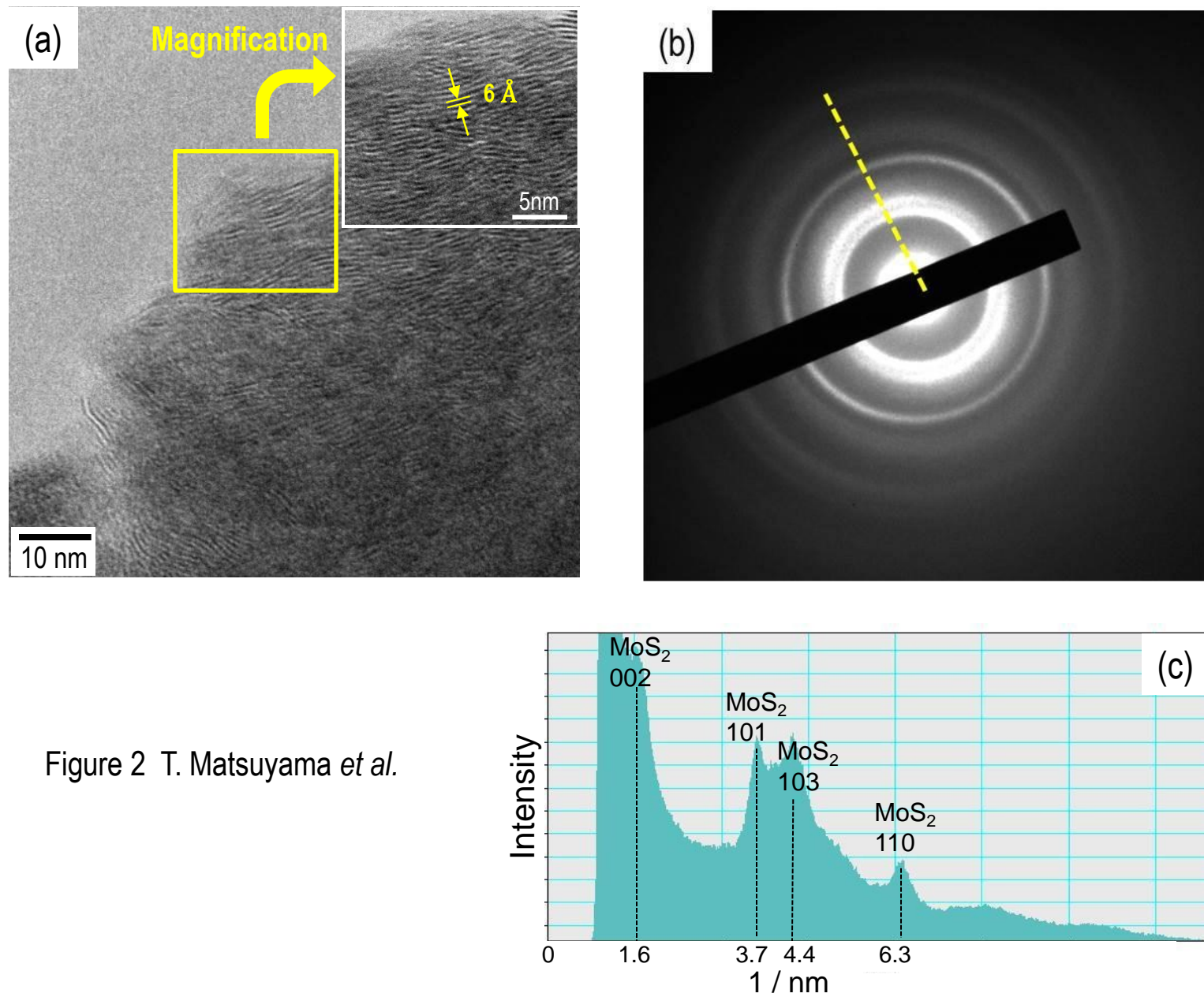
Figure 2 High-resolution TEM image (a), electron diffraction pattern (b) and its intensity profile (c) of the molybdenum sulfide prepared by milling for 80 h. The inset in (a) shows magnified image of (a).

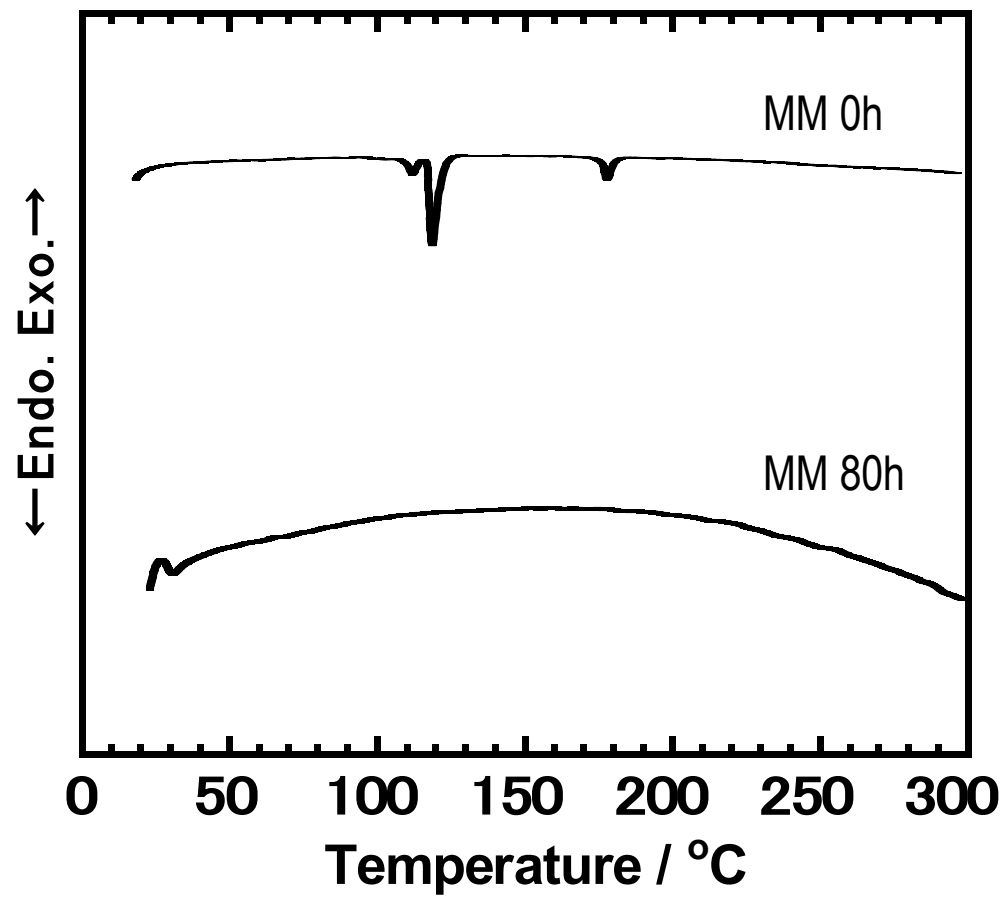
Figure 3 DTA curves of the mixture and product of Mo metal and sulfur prepared by MM for 0 and 80 hours.

Figure 4 SEM images of the mixture and product of Mo metal and sulfur prepared by MM for 0 and 80 hours.

Figure 5 Charge-discharge curves (a) and rate performance (b) of the all-solid-state cells with amorphous MoS₃ and crystalline MoS₂.

Figure 1 T. Matsuyama *et al.*

Figure 2 T. Matsuyama *et al.*

Figure 3 T. Matsuyama *et al.*

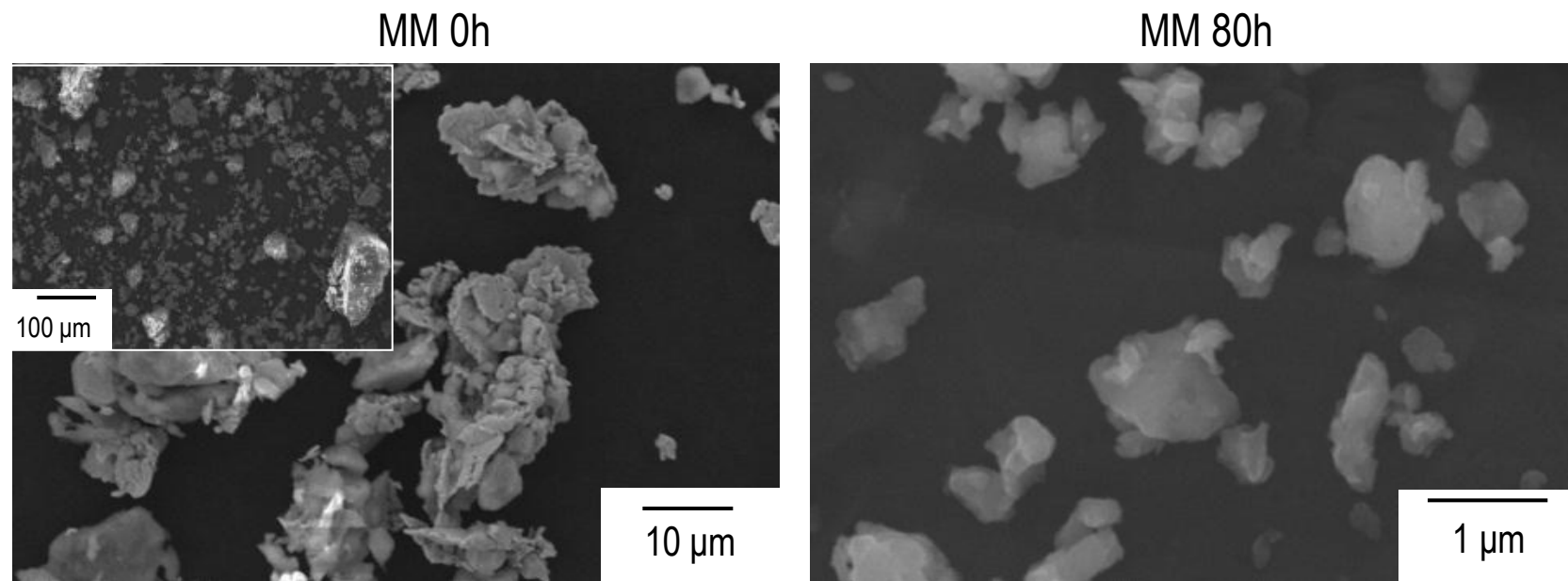


Figure 4 T. Matsuyama *et al.*

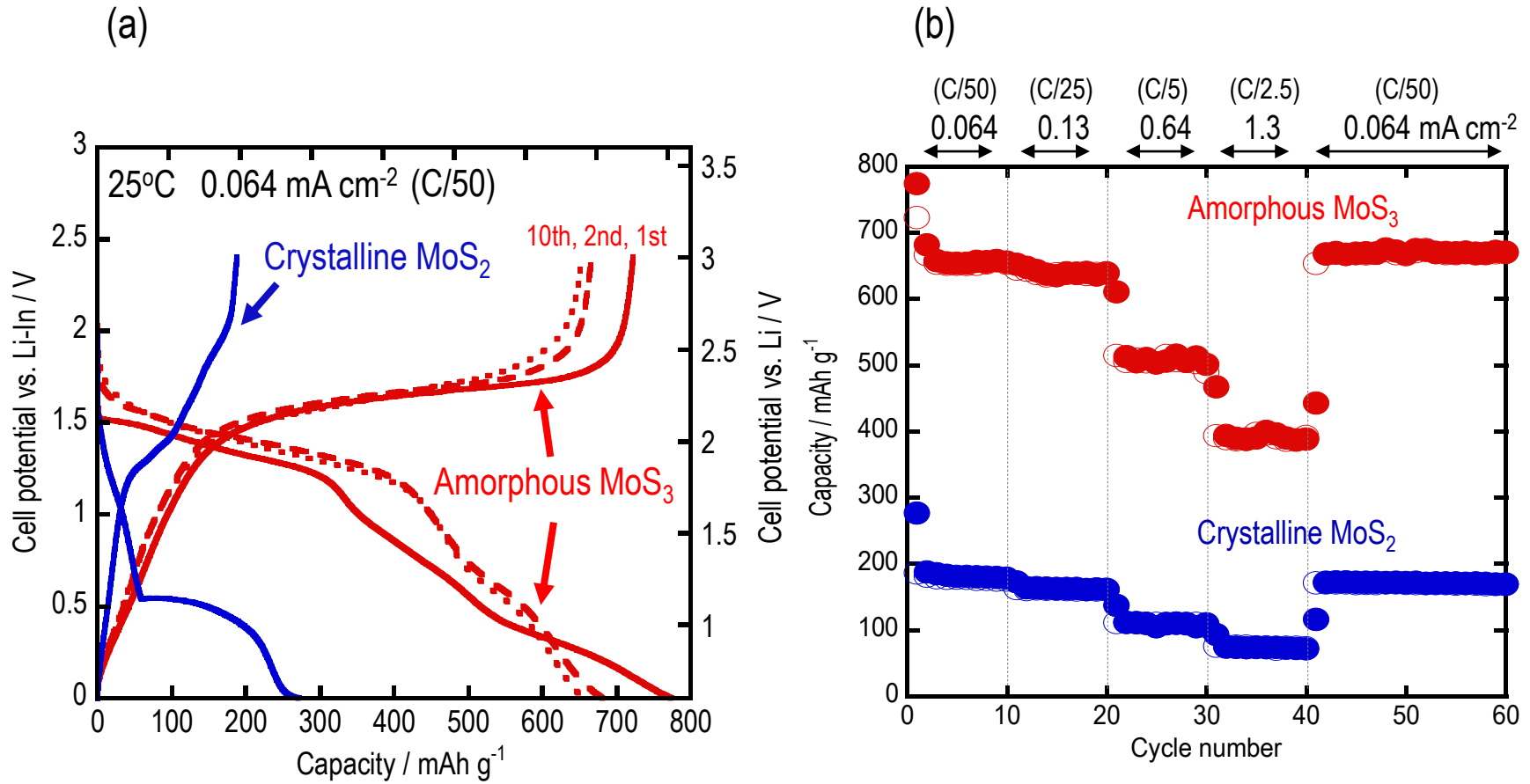
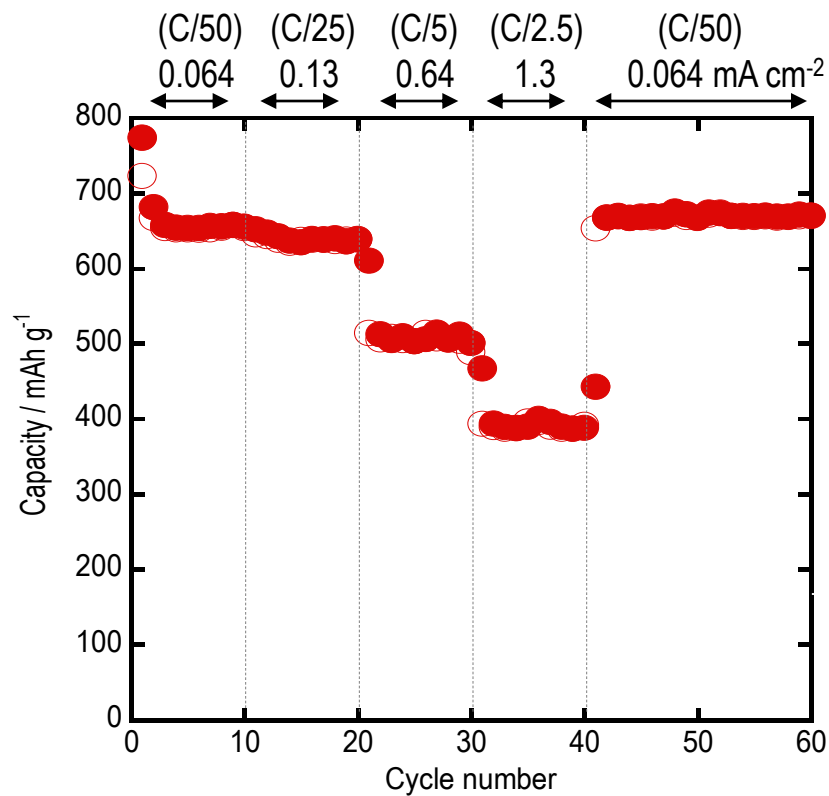
Figure 5 T. Matsuyama *et al.*

Table of contents



The all-solid-state lithium batteries with amorphous MoS₃ showed the high reversible capacities for 60 cycles.